ASTRONOMY & ASTROPHYSICS
SUPPLEMENT SERIES

Astron. Astrophys. Suppl. Ser. **145**, 71–82 (2000)

Line-of-sight velocity distributions of 53 early-type galaxies⋆

W. Koprolin and W.W. Zeilinger

Institut für Astronomie der Universität Wien, Türkenschanzstraße 17, A-1180 Wien, Austria

Received December 1, 1999; accepted April 20, 2000

Abstract. 55 long-slit spectra of 53 early-type galaxies were observed at La Silla/ESO and reduced using standard methods. The line-of-sight velocity distributions (LOSVDs) were measured using the fourier quotient method and the fourier fitting method as described by van der Marel et al. (1993). 32% of the examined galaxies contain kinematically decoupled stellar omponents, the size of these cores was 0.40 ± 0.28 kpc, in each case the core was smaller than 1 kpc. Analysis of the kinematics reveals in 49% of the sample galaxies the signature of a stellar disk component, in 15% this is uncertain. There is evidence that the phenomenon of kinematically decoupled components is present in the whole class of early-type galaxies. Several correlations between photometric and kinematic parameters like the $(v/\sigma)^*$ vs. ϵ diagram, the anisotropy – luminosity correlation or κ-space were as well examined using measurement results for spectroscopic data and photometric data out of literature. It is also shown that those sample galaxies with kinematically decoupled components are more likely to be found in groups of high density, strengthening the assumption that such components are remnants of merging events.

Key words: galaxies: elliptical and lenticular — galaxies: fundamental parameters — galaxies: kinematics and dynamics

1. Introduction

The traditional picture of describing elliptical galaxies as simple isothermal bodies which are chemically well mixed has dramatically changed. Ellipticals are now seen as complex systems from the photometrical, kinematical and chemical point of view. The properties of ellipticals are found to correlate with their mass (Burstein et al. 1997). Large ellipticals are triaxial systems supported by anisotropic velocity distributions of the stars. Low-luminosity systems are on the contrary generally axisymmetric rotationally supported bodies.

One of the most noteable features observed in ellipticals are kinematically decoupled core components. The most extreme cases are peculiar cores which are characterized by angular momentum vectors which are opposite or perpendicular with respect to the main body of the galaxy. Merging seems to be a plausible explanation for the origin of the decoupled component. This is also supported by the fact that the metallicities of the core component as measured through the absorption line indices appear to be enhanced with respect to the rest of the galaxy (Bender & Surma 1992). In about 30% of the nearby luminous ellipticals peculiar core kinematics are detected. Taking however projection effects into account, it is estimated that more than 50% of all luminous ellipticals should contain a kinematically decoupled core (Bender 1996).

In order to study the stellar kinematical properties of ellipticals *in a homogenous manner*, we carried out a spectroscopic study of a sample of 53 southern ellipticals. In the following section we summarize the observations and data reduction. In Sect. 3 we present the results obtained by application of the fourier fitting method as described by van der Marel & Franx (1993). The correlations between global photometric and kinematic properties are discussed in Sect. 4. Finally we discuss some conclusion on the merging history of the class of elliptical galaxies which can be drawn on the basis of the sample.

2. Observations and data reduction

In alltogether 15 nights 55 long-slit spectra of 53 early-type galaxies were obtained using the ESO 1.52 m telescope equipped with a B&C Cassegrain spectrograph. The observation log is given in Table 2. The parameters of the instrumental setups are described in Table 3. Instrumental dispersions for the different setups were determined by measuring the width of night-sky emission

Send offprint requests to: W. Koprolin

⋆ Full Fig. 6 is only available at http://www.edpsciences.org

lines and helium-argon lines in the calibration spectra. The seeing was typically $1.5-2$ arcsec. The detectors employed were all Ford Aerospace 2048×2048 pixel CCDs with a pixel size of 15×15 μm^2. The position angle of the slit was generally aligned with the optical major axis of the target galaxy.

The integration times range from 40 to 120 min. The observed sample contains little less than half of all early-type galaxies with systemic velocities < 3000 km s^{-1}. Exceptions are NGC 3302 ($v_{\rm sys} = 4075$ km s^{-1}) and NGC 3309 ($v_{\rm sys} = 4057$ km s^{-1}). Table 1 lists the sample galaxies and their basic parameters.

The spectra were calibrated with the ESO images processing package MIDAS using standard procedures for bias subtraction and flat field correction. Artifacts produced by cosmic ray events were removed by applying a filtering algorithm and by visual inspection. The science spectra were bracketed by helium-argon calibration spectra in order to verify shifts along the dispersion due to instrumental flexure. No significant shifts were however detected. Wavelength calibration was performed on the science frames for each spectral row independently by fitting a third order polynomial, using the respective averaged helium-argon spectra as reference. The rms error of the dispersion curve was typically < 0.4 Å. A sky spectrum was derived for each galaxy spectrum by fitting each wavelength bin with a first order polynomial at the border regions of the frame uncontaminated by the contribution of the galaxy light. To obtain an acceptable S/N all over the spectra, several lines in spatial direction were averaged until $S/N > 12$ was reached, where necessary. Within the central 3 arcsec of the galaxies $S/N \approx 35$ is typical.

For the subsequent analysis of the stellar kinematics the fourier fitting method using Gauss-Hermite polynomials was used as described by van der Marel et al. (1993). Spectra of non-rotating K and M giants obtained in the same instrumental setup as the galaxy spectra were used as velocity templates. Typically 4 to 8 such template stars were observed in each observing run.

3. Results

Emission lines were detected in 5 galaxies of the sample: UGC 4508, NGC 1889, NGC 3125, NGC 5237 and UGC 7354. Table 4 lists the detected emission lines of the respective galaxies and their properties. Analysis suggests photoionisation to be the main cause for the line emission, which is typical for H II regions.

The results for the stellar kinematics obtained for all 49 sample galaxies with absorption lines strong enough for fourier fitting are presented in the Appendix. The radial velocity and velocity dispersion profiles compare favorably with previously published measurements (Bender et al. 1994; Davies et al. 1983; Franx et al. 1989; Binney et al. 1990; Carollo & Danziger 1994a). The agreement of the kinematical profiles is for the major part within 1σ deviation. For most of the galaxies of our sample no published h_3 and h_4 are available for comparison.

Notes on individual objects:

IC 1729: Asymmetric radial velocity profile, central depression in the velocity dispersion profile.

NGC 1404: Disk without rotation within 0.1 $r_{\rm e}$, velocity profile constant within 1 $r_{\rm e}$, $h_3 \propto -v$: typical example of decoupled central component kinematics.

UGC 4508: cE? High-intensity emission lines, low continuum.

NGC 1889: In interaction with the disklike galaxy NGC 1888, merger. The kinematic profiles overlap, resulting in a velocity dispersion profile and line strength increase outward. Hα and [N II] line emission were detected, possibly from the neighboring galaxy. Liu & Kennicutt (1995) state NGC 1888 to be a spiral of the type Sa or Sb with dominent old stellar population and only weak line emission.

NGC 2663: Very small rotation, unusually high velocity dispersion. This galaxy is a massive brightest cluster member and characterized by very anisotropic dynamics (Carollo & Danziger 1994b). The galaxy also features a compact central radio source (Danziger & Goss 1983; Sadler et al. 1989).

NGC 2271: Kinematically decoupled central component within 1.5″ of the galaxy's center without rotation.

NGC 3078: Slightly asymmetric kinematically decoupled central component without rotation, also supported by a central depression in the Mg_2 profile (Carollo et al. 1993).

NGC 3125 = AM 1004-294: High intensity emission lines, low continuum. This is a bright, compact low-redshift galaxy in a cluster with regular outer isophotes and double knots, it is classified as an amorphous H II galaxy (Telles et al. 1997) or a blue compact dwarf (Marlowe et al. 1997).

NGC 3136: Counter-rotation disk 4″ away from the center of intensity with a diameter of 2″; significance is low.

NGC 3250: Counter-rotating disk 9″ away from the center of intensity with a diameter of 3″, $h_3 \propto -v$, indicating decoupled central component kinematics (Bender et al. 1994). The Mg_2 profile of this galaxy also features a central depression (Carollo et al. 1993).

NGC 3268: This galaxy features rotation only at one side of the core probably due to the presence of dust. It also has a parsec-scale radio core (Slee et al. 1994). $h_3 \propto v$, indicating a disk component (Bender et al. 1994).

NGC 3302: Dust lane along major axis.

NGC 3557B: Possible kinematically decoupled central component supported by the asymmetric rotational velocity profile and $h_3 > 0$, low significance because of low spatial resolution.

NGC 3636: E0 with low velocity dispersion ($\sigma < 160$ km s^{-1}).

Table 1. Programme galaxies and their basic parameters

Object (PGC[1])	Object (NGC/IC/UGC)	Type (RC3[2])	Type (RSA[3])	Type (PGC)	B_T^0 (ESO-Uppsala[4])	A_e	V_{hel}
6588	IC 1729	SAB0$^-$:		E	13.28	29.8	1495
13433	NGC 1404	E1	E2	E	10.89	26.7	1925
13609	NGC 1427	cD	E5	E	11.76	32.9	1430
14695	NGC 1537	SAB0$^-$ pec?	E6	LB	11.53	26.1	1371
14757	NGC 1549	E0	E2	E	10.58	47.5	1153
17196	NGC 1889	cD pec:		E M	14.1		2472
19476	NGC 2271	SAB0$^-$		LB	12.11	64.3	2588
20047	NGC 2325	E4	E4	E	10.96	86.5	2248
20916	NGC 2380	SAB0:		LB	10.38	43.4	1775
21325	NGC 2434	E0	E0	E	11.43	40.5	1327
23304	IC 2311	E0:		E	11.00	17.7	1836
24352	UGC 4508	cE ?		S	14.90		1917
24590	NGC 2663	E		E	10.23	84.6	2048
25075	NGC 2699	E:		E	13.57		1825
26592	NGC 2887	SA0(s)$^-$?		L	11.72	27.4	2850
26601	NGC 2865	E3	E4	E	12.29	11.7	2581
26733	NGC 2872	E2		E	12.64	20.8	3226
26768	NGC 2888	cD:	E2	E	12.98	14.7	2233
27885	NGC 2986	E2	E2	E	11.51	41.4	2264
28806	NGC 3078	E2	E3	E	11.93	23.8	2506
28845	NGC 3087	cD:	E2	E	12.34	16.1	2662
29311	NGC 3136	E:	E4	E	11.23	41.4	1647
29366	NGC 3125	E ?	Amorphous	E	13.16	9.2	1080
30314	NGC 3224	cD		E	12.48	15.3	3088
30671	NGC 3250	E4	E3	E	11.67	32.1	2883
30859	NGC 3258	E1	E1	E	12.27	27.4	2808
30875	NGC 3260	E pec:		E	13.06	25.0	2413
30949	NGC 3268	E2	E2	E	12.23	36.1	2761
31391	NGC 3302	SA0		L	13.16	20.4	4075
31466	NGC 3309	E3	E1	E	12.34	31.4	4057
32249	NGC 3377	E5	E6	E	11.13	33.7	689
33824	NGC 3557B	E5:		E M	12.92		2855
33871	NGC 3557	E3	E3	E	11.13	37.8	3014
34160	NGC 3585	E7	E7/S0$_1$(7)	E	10.53	39.5	1491
24513	NGC 3617	cD			13.26	11.9	1491
34709	NGC 3636	E0		E	13.19		1715
36918	NGC 3904	E2:	E2	E	11.67	23.3	1750
37061	NGC 3923	E4	E4/S0$_1$(4)	E	10.52	53.3	1607
37863	NGC 4033	E6	S0$_1$(6)	E	12.52	16.1	1521
38411	NGC 4105	E3	S0$_{1/2}$(3)	E M	11.21	41.4	1900
38417	NGC 4106	SB0(s)$^+$	SB0/a (tides)	LB	11.88	61.0	2189
39628	UGC 7354			E	14.66		1684
39659	NGC 4261	E2	E3	E	11.32	28.6	2200
43276	NGC 4697	E6	E6	E	10.03	75.4	1210
46330	NGC 5061	E0	E0	E	11.06	25.5	2065
48139	NGC 5237	I0 ?		E M	12.84	26.9	321
54646	NGC 5903	E2	E3/S0$_1$(3)	E	11.76	35.2	2519
62589	IC 4797	cD pec:	E5/S0$_1$(5)	E	12.04	17.7	2582
64136	NGC 6861	SA0(s)$^-$:	S0$_3$(6)	LB	11.78	22.8	2819
66318	NGC 7029	E6:	S0$_1$(5)	E	12.26	24.4	2818
66549	NGC 7049	SA(s)0	S0$_3$(4)/Sa	L	11.42	47.8	2198
68020	NGC 7196	E:	E3/S0$_3$(3)	E	12.31	21.7	3007
70975	IC 5297			S	15.6		

[1] Paturel et al. 1989.
[2] de Vaucouleurs et al. 1991.
[3] Sandage & Tammann 1981.
[4] Lauberts & Valentijn 1989.

Table 2. Observation log

observing run	date	galaxy	integration time	position angle
1991	Mar. 24/25	NGC 3302	7200 s	28°
		NGC 4697	3600 s	80°
	Mar. 25/26	NGC 3309	7200 s	170°
	Mar. 26/27	NGC 4105	7200 s	115°
		NGC 4106	7200 s	115°
1992	Jan. 29/30	NGC 1537	2×2400 s	94°
		NGC 2325	2×2400 s	6°
		NGC 2663	2×2400 s	113°
		NGC 3078	2400 s	15°
		NGC 3268	2400 s	62°
	Jan. 30/31	NGC 2271	2×2400 s	91°
		NGC 2865	2×2400 s	128°
		NGC 3087	2×2400 s	126°
		NGC 3136	2×2400 s	126°
	Jan. 31/Feb. 1	NGC 1549	2×2400 s	4°
		NGC 3250	2×2400 s	136°
		NGC 3258	2×2400 s	55°
	Feb. 1/2	NGC 1427	2×2400 s	77°
		NGC 2380	2×2400 s	72°
		NGC 3224	2×2400 s	134°
		NGC 3585	2×2400 s	96°
		NGC 3904	2400 s, 1200 s	0°
	Feb. 2/3	NGC 2888	2×2400 s	170°
		NGC 2434	2×2400 s	126°
		NGC 2887	2×2400 s	87°
		NGC 5061	1800 s, 1500 s	95°
1992	Aug. 25/26	NGC 5903	2×2700 s	139°
		IC 4797	2×2700 s	145°
		NGC 7029	2×2700 s	69°
		NGC 7196	2×2700 s	47°
		IC 1729	2700 s	142°
		NGC 1404	2700 s	160°
	Aug. 26/27	NGC 7049	2×3600 s	57°
	Aug. 28/29	NGC 6861	3600 s	140°
1993	Feb. 16/17	IC 2311	3600 s	84°
		NGC 2699	3600 s	50°
		NGC 2986	3600 s	78°
		NGC 3377	3600 s	36°
		NGC 3923	3600 s	50°
	Feb. 17/18	NGC 1889	3600 s	161°
		NGC 3125	3600 s	111°
		IC 5297	3600 s	0°
		NGC 3617	3600 s	147°
		NGC 4033	3600 s	47°
		NGC 4261	3600 s	160°
	Feb. 18/19	NGC 2663	3600 s	98°
		NGC 2872	3600 s	32°
		NGC 3260	3600 s	0°
		NGC 3557B	3600 s	107°
		NGC 3557	3600 s	30°
		NGC 4697	3600 s	160°
	Feb. 19/20	UGC 4508	5400 s	90°
		NGC 3636	3600 s	90°
		UGC 7354	5400 s	19°
		NGC 5237	3600 s	128°

Table 3. Observation parameters

date	CCD ESO-number	spatial resolution [arcsec/pixel]	grating ESO-number	wavelength range [Å]	slit width [arcsec]	spectral resolution [Å/pixel]	instrumental dispersion [km s^{-1}]
1991 Mar. 24 – 25	13	0.81	25	4253−6836	2.0	2.788	169
1991 Mar. 25 – 28	13	0.81	10	4835−5735	1.7	0.974	51
1992 Jan. 29 – Feb. 3	27	0.81	10	5162−6659	2.0	0.970	53
1992 Aug. 25 – 29	27	0.81	10	5175−6687	2.0	0.969	39
1993 Feb. 16 – 20	24	0.81	10	5175−6687	2.0	0.969	39

Table 4. Measured emission lines of the sample galaxies

galaxy	element	λ_0 [Å]	λ [Å]	$FWHM$ [Å]	v [km s^{-1}]	σ [km s^{-1}]
UGC 4508	Fe II	5591.38	5626.0	2.0	1856.2	44
	Fe I	5595.06	5630.1	2.3	1877.5	50
	He I	5875.6	5912.1	2.1	1862.4	43
	[N II]	6548.1	6588.7	2.3	1858.8	43
	Hα	6562.8	6603.4	(4.6)	1854.6	(85)
	[N II]	6583.4	6624.2	2.4	1859.3	44
NGC 1889	[N II]	6548.1	6603.2	5.0	2522.6	96
	Hα	6562.8	6617.62	3.0	2504.2	56
	[N II]	6583.4	6638.7	5.0	2518.2	95
NGC 3125	Fe II	5591.38	5611.9	2.2	1100.2	48
	Fe I	5595.06	5615.8	2.2	1111.3	48
	He I	5875.6	5896.73	2.5	1078.1	52
	Fe II	6149.238	6171.83	2.6	1101.4	52
	[N II]	6504.9	6528.552	2.7	1090.1	51
	[N II]	6548.1	6571.7	2.6	1080.5	48
	Hα	6562.8	6586.44	2.73	1079.9	50.7
	[N II]	6583.4	6607.26	2.6	1086.5	48
NGC 5237	[N II]	6548.1	6555.2	(6.1)	325.1	(114)
	Hα	6562.8	6570.07	2.3	332.1	42
	[N II]	6583.4	6590.7	2.4	332.4	45
UGC 7354	Fe II	5619.9	5591.38	2.0	1529.2	44
	Fe I	5623.9	5595.06	2.2	1545.3	48
	Fe I	5832.69	5804.06	1.9	1478.8	40
	Fe III	5862.67	5833.65	2.8	1491.3	59
	Fe II	6180.79	6149.238	2.2	1538.2	44
	[O I]	6332.27	6300.3	2.1	1521.3	41
	[N II]	6538.16	6504.9	2.4	1532.9	45
	[N II]	6581.43	6548.1	2.2	1526.0	41
	Hα	6595.7	6562.8	(5.3)	1502.9	(99)
	[N II]	6616.878	6583.4	2.47	1524.5	45.9

NGC 3904: Rotation disk ($r < 6''$) within the center, $h_3 \propto -v$, indicating decoupled central component kinematics.

NGC 4105, NGC 4106 = AM 1204-292: Gravitational interaction, reciprocal influence of kinematics. NGC 4105 features decoupled fast rotation within $2''$ of the galaxy's center, supported by the fact that h_3 resambles $-v$; NGC 4106 has an asymmetric rotational velocity profile and $h_3 > 0$. The latter is classified as lenticular in the ESO-Uppsala Sky Survey with a diffuse, round arm clearly visible, possibly produced by the interaction. RC3 classifies it for this reason as SBb, however the color is more consistent with an S0 (Reduzzi & Rampazzo 1996).

NGC 4697: Large E6 galaxy with only slight rotation, it also features a dust lane of intrinsically circular shape, located in the equitorial plane. The galaxy is flattened and may be an S0, the spheroidal part of NGC 4697 may well be a large bulge (Dejonghe et al. 1996).

NGC 5237 = AM 1334-423: Nearby irregular galaxy, high-intensity emission lines, low continuum. This galaxy is believed to be a remnant of a spiral which collided with Centaurus A (NGC 5128) 5 10^8 yr ago, lost half its disk material, which now forms the conspicuous ring of gas and dust line in Centaurus A, and was ejected as a non-rotating shred of dusty, gas-rich disc material which appears as a blue irregular/starburst dwarf galaxy

(Thomson 1992).
NGC 6861 = IC 4949: Unusually high velocity dispersion at the center, fast rotation. This is a massive S0 galaxy, possibly influenced by a bar component. This galaxy also features a compact radio source in its core (Slee et al. 1994).
UGC 7354 = A 1216+04: Only emission lines, no absorption lines detected. This is a blue compact dwarf (Papaderos et al. 1996) or a starburst galaxy (Campos-Aguilar & Moles 1991).

The ESO-Uppsala Sky Survey designates 25 galaxies as cluster members, 8 galaxies as group members, 3 galaxies as pairs (NGC 4105 with NGC 4106, NGC 5237 with a compact object) and 6 galaxies as field galaxies (IC 4797, NGC 2380, NGC 2865, NGC 2887, NGC 3302, NGC 3585). For 12 galaxies no such data was available.

Table 5 contains the most important measured or derived spectroscopic quantities of the sample galaxies. These mean parameters describe the individual galaxies sufficiently well for the investigation of correlations between different kinematic and non-kinematic properties and LOSVDs. All mean parameters refer to the galaxy properties within their effective radii.

- $v_{\rm sys}$ is the heliocentric corrected system velocity;
- $v_{\rm rot}$ is the rotational velocity, it was measured as the difference between an average of the radial velocities where the rotation curve flattened and the central velocity;
- $\mathrm{d}v/\mathrm{d}r_0$ is the gradient of the rotation curve at the center of the galaxy;
- σ_0 is the mean value of all velocity dispersions within 5 arcsec[5] of the galaxy's center;
- $\sigma_{\rm m}$ was derived by averaging all velocity dispersions within $r_{\rm e/2}$[6];
- $\sigma_{\rm e/2}$ is the velocity dispersion at half of the effective radius;
- $\Delta\sigma_{\rm e/2}$ is the relative change of the velocity dispersion and is calculated as $\Delta\sigma_{\rm e/2} = (\sigma_{\rm e/2} - \sigma_0)/\sigma_0$;
- $(v/\sigma)^*$ is the anisotropy parameter and is calculated as $(v/\sigma)^* = \frac{(v/\sigma)_{\rm observed}}{(v/\sigma)_{\rm oblate}}$, where $(v/\sigma)_{\rm oblate} = \sqrt{\frac{\epsilon}{1-\epsilon}}$. The ellipticities of the sample galaxies were taken from RC3.

4. Correlations between kinematic and photometric parameters

The photometric parameters used for these correlation were taken from Burstein et al. (1987), RC3 and the ESO-Uppsala Sky Survey, kinematic quantities are results of this work.

[5] Consistent with Faber et al. (1989).
[6] Consistent with Bender et al. (1994).

To calculate the distances of the sample galaxies two different models were used:

1. The distances were calculated by assuming an undisturbed Hubble-flow and $H_0 = 75$ km s^{-1} Mpc^{-1}, using the system velocities taken from Faber et al. (1989).
2. The distances were taken from the catalogue of Kraan-Korteweg (1986), where a model of the Virgo cluster infall was added to the Hubble flow.

4.1. Correlations between anisotropy and photometric parameters

Binney (1978) was the first to utilize a (v/σ) vs. ϵ-diagram in order to get a statistic reference if a group of galaxies suits into the model of an oblate rotator or whether it rather consists of dynamical hot systems, where chaotic star motion dominates.

In Fig. 1 $(v/\sigma)^*$ vs. ϵ, (v/σ) vs. ϵ and v vs. ϵ are plotted for all sample galaxies where these parameters are available. Galaxies with $(v/\sigma)^* > 1$ are expected to be rotationally supported systems. These are (sorted by increasing ϵ): NGC 1404, NGC 2872, NGC 3260, NGC 4105, NGC 7196, NGC 3557, NGC 3268, NGC 6861, NGC 2271, NGC 7049 and NGC 1537. The last four objects are S0 systems, the others are elliptical galaxies with fast rotation.

The correlation between anisotropy and luminosity was first described in Davies et al. (1983). Galaxies with low luminosity are mostly rotationally supported systems while galaxies with high luminosity are generally systems with high anisotropy. The existence of this correlation is explained by the increasing influence of chaotic relaxation and the increasing influence of merging with increasing galaxy mass (and therefore luminosity) (Davies et al. 1983; Bender et al. 1992). In Fig. 2 the correlation between $(v/\sigma)^*$ and M_B is plotted.

The galaxy NGC 3557 is represented by the data point with the greatest luminosity and doesn't follow the general trend. This E3-galaxy features high luminosity and a rotational velocity of $v_{\rm rot} = 217 \pm 11$ km s^{-1}.

4.2. κ-space

κ-space was introduced by Bender et al. (1992) and was originally defined to examine the physical properties of dynamically hot galaxies. The axes of κ-space are proportional to the logarithm of galaxy mass (κ_1), mass-to-light ratio (κ_3), and a third quantity that is mainly surface brightness (κ_2) (Burstein et al. 1997). The κ_1/κ_3-projection represents a side-view of the fundamental plane, the κ_1/κ_2-projection shows it nearly face-on.

All sample galaxies where the necessary input parameters $\sigma_{\rm c}$, $R_{\rm e}$ and $I_{\rm e}$ were available are represented in Fig. 3.

Table 5. Measured spectroscopic parameters of the sample galaxies. Quantities marked with * are results of emission line measurements

galaxy	$v_{\rm sys}$ [km s^{-1}]	$v_{\rm rot}$ [km s^{-1}]	dv/dr_0 [km s^{-1} arcsec^{-1}]	σ_0 [km s^{-1}]	$\sigma_{\rm m}$ [km s^{-1}]	$\sigma_{\rm e/2}$ [km s^{-1}]	$\Delta\sigma_{\rm e/2}$	$(v/\sigma)^*$
I1729	1441 ± 3	54 ± 4	21 ± 8	131 ± 7	130 ± 9	127 ± 18	−0.03 ± 0.14	0.45 ± 0.05
N1404	1834 ± 4	113 ± 10	1 ± 9	259 ± 5	247 ± 4	216 ± 10	−0.17 ± 0.04	1.30 ± 0.11
N1427	1417 ± 3	63 ± 10	9 ± 5	157 ± 4	150 ± 8	150 ± 8	−0.05 ± 0.06	0.61 ± 0.10
N1537	1407 ± 2	176 ± 8	18 ± 4	138 ± 4	121 ± 4	102 ± 11	−0.26 ± 0.08	2.03 ± 0.11
N1549	1198 ± 2	53 ± 12	0 ± 3	218 ± 3	191 ± 4	109 ± 11	−0.50 ± 0.05	0.61 ± 0.14
N1889	2406 ± 6	113 ± 13	9 ± 18	167 ± 11	—	—	—	—
	2524 ± 8*	—	—	89.4 ± 19.5*	—	—	—	—
N2271	2558 ± 6	263 ± 36	20 ± 7	237 ± 7	228 ± 8	235 ± 8	−0.01 ± 0.04	1.72 ± 0.24
N2325	2073 ± 5	9 ± 17	5 ± 17	206 ± 8	215 ± 13	179 ± 27	−0.13 ± 0.13	0.05 ± 0.09
N2380	1755 ± 4	68 ± 16	4 ± 10	200 ± 6	—	—	—	—
N2434	1358 ± 4	41 ± 15	7 ± 10	189 ± 6	170 ± 8	152 ± 10	−0.20 ± 0.06	0.89 ± 0.33
I2311	1636 ± 4	30 ± 18	7 ± 8	211 ± 5	189 ± 5	143 ± 13	−0.32 ± 0.07	0.50 ± 0.30
U4508	1865 ± 8*	—	—	44.9 ± 3.1*	—	—	—	—
N2663 (major axis)	1987 ± 8	35 ± 31	6 ± 19	329 ± 11	—	—	—	—
N2663 (PA=98°)	1951 ± 8	13 ± 19	3 ± 13	321 ± 9	—	—	—	—
N2699	1715 ± 3	73 ± 6	17 ± 5	152 ± 6	—	—	—	—
N2887	2843 ± 6	6 ± 20	2 ± 19	296 ± 8	267 ± 7	187 ± 9	−0.37 ± 0.04	0.03 ± 0.12
N2865	2529 ± 4	72 ± 15	1 ± 10	184 ± 5	182 ± 5	175 ± 8	−0.05 ± 0.05	0.67 ± 0.14
N2872	3117 ± 9	190 ± 50	8 ± 16	281 ± 13	248 ± 10	154 ± 29	−0.45 ± 0.11	1.98 ± 0.53
N2888	2342 ± 3	54 ± 9	14 ± 6	138 ± 7	140 ± 7	141 ± 9	0.02 ± 0.08	0.65 ± 0.11
N2986	2174 ± 7	57 ± 12	30 ± 10	282 ± 13	243 ± 14	206 ± 31	−0.27 ± 0.11	0.61 ± 0.13
N3078	2428 ± 5	99 ± 8	30 ± 18	305 ± 6	292 ± 9	255 ± 16	−0.16 ± 0.05	0.75 ± 0.06
N3087	2511 ± 4	34 ± 8	13 ± 5	259 ± 6	246 ± 7	192 ± 24	−0.26 ± 0.10	0.30 ± 0.07
N3136	1670 ± 5	10 ± 16	2 ± 16	226 ± 5	197 ± 5	115 ± 12	−0.49 ± 0.06	0.07 ± 0.12
N3125	1077 ± 11*	—	—	51.9 ± 4.0*	—	—	—	—
N3224	2898 ± 8	94 ± 26	25 ± 10	216 ± 16	206 ± 13	172 ± 19	−0.20 ± 0.11	0.94 ± 0.26
N3250	2704 ± 5	132 ± 9	21 ± 10	298 ± 6	262 ± 6	188 ± 16	−0.37 ± 0.06	0.81 ± 0.06
N3258	2646 ± 5	39 ± 9	14 ± 14	357 ± 6	319 ± 6	267 ± 18	−0.25 ± 0.05	0.29 ± 0.07
N3260	2248 ± 6	211 ± 16	39 ± 12	174 ± 9	147 ± 10	106 ± 24	−0.39 ± 0.14	2.71 ± 0.27
N3268	2575 ± 6	211 ± 38	47 ± 21	197 ± 10	177 ± 10	122 ± 17	−0.38 ± 0.09	1.91 ± 0.36
N3302	3742 ± 10	18 ± 41	12 ± 15	379 ± 17	309 ± 21	148 ± 21	−0.61 ± 0.06	0.10 ± 0.22
N3309	4024 ± 6	17 ± 10	12 ± 9	282 ± 10	—	—	—	—
N3377	591 ± 2	86 ± 4	25 ± 7	135 ± 7	115 ± 8	81 ± 22	−0.40 ± 0.17	0.88 ± 0.07
N3557B	2723 ± 4	124 ± 7	32 ± 11	201 ± 6	—	—	—	—
N3557	2885 ± 7	217 ± 11	26 ± 7	363 ± 14	276 ± 7	181 ± 17	−0.50 ± 0.05	1.26 ± 0.07
N3585	1333 ± 2	157 ± 3	19 ± 4	232 ± 3	218 ± 3	220 ± 8	−0.06 ± 0.04	0.80 ± 0.02
N3617	1955 ± 3	99 ± 20	9 ± 4	111 ± 8	111 ± 7	109 ± 20	−0.02 ± 0.20	1.40 ± 0.30
N3636	1609 ± 4	8 ± 14	4 ± 6	114 ± 10	—	—	—	—
N3904	1592 ± 3	69 ± 7	18 ± 5	211 ± 4	195 ± 5	118 ± 14	−0.44 ± 0.07	0.57 ± 0.06
N3923	1639 ± 4	53 ± 13	4 ± 10	290 ± 4	275 ± 6	176 ± 22	−0.39 ± 0.08	0.27 ± 0.07
N4033	1452 ± 3	99 ± 8	10 ± 6	134 ± 4	142 ± 4	161 ± 12	0.20 ± 0.10	0.60 ± 0.05
N4105	2147 ± 3	158 ± 14	19 ± 8	181 ± 4	165 ± 4	133 ± 6	−0.27 ± 0.04	1.62 ± 0.15
N4106	1861 ± 4	10 ± 5	9 ± 11	230 ± 5	216 ± 6	169 ± 9	−0.27 ± 0.04	0.09 ± 0.05
U7354	1505 ± 18*	—	—	46.1 ± 4.9*	—	—	—	—
N4261	2038 ± 5	12 ± 16	1 ± 13	356 ± 5	294 ± 4	224 ± 14	−0.37 ± 0.04	0.12 ± 0.16
N4697 (PA=100°)	1050 ± 3	97 ± 7	27 ± 4	187 ± 6	172 ± 9	164 ± 12	−0.12 ± 0.07	0.77 ± 0.07
N4697 (minor axis)	1088 ± 3	27 ± 10	6 ± 4	181 ± 4	174 ± 4	177 ± 11	−0.02 ± 0.06	0.21 ± 0.08
N5061	1931 ± 3	59 ± 13	2 ± 7	220 ± 4	213 ± 4	229 ± 13	0.04 ± 0.06	0.66 ± 0.15
N5237	302 ± 3*	—	—	48.5 ± 1.0*	—	—	—	—
N5903	2528 ± 4	9 ± 17	4 ± 11	212 ± 6	194 ± 6	177 ± 16	−0.16 ± 0.08	0.08 ± 0.17
I4797	2635 ± 3	137 ± 6	28 ± 9	245 ± 5	219 ± 4	159 ± 12	−0.35 ± 0.05	0.56 ± 0.03
N6861	2752 ± 7	240 ± 10	45 ± 11	382 ± 7	340 ± 6	297 ± 19	−0.22 ± 0.05	0.96 ± 0.04
N7029	2703 ± 5	132 ± 7	29 ± 6	201 ± 7	177 ± 6	106 ± 12	−0.48 ± 0.06	0.82 ± 0.05
N7049	2183 ± 5	171 ± 17	20 ± 12	267 ± 7	220 ± 7	114 ± 23	−0.57 ± 0.09	1.16 ± 0.12
N7196	2800 ± 7	243 ± 25	40 ± 18	260 ± 12	234 ± 9	229 ± 24	−0.12 ± 0.10	1.76 ± 0.19
I5297	2831 ± 6	113 ± 25	5 ± 19	267 ± 7	—	—	—	—

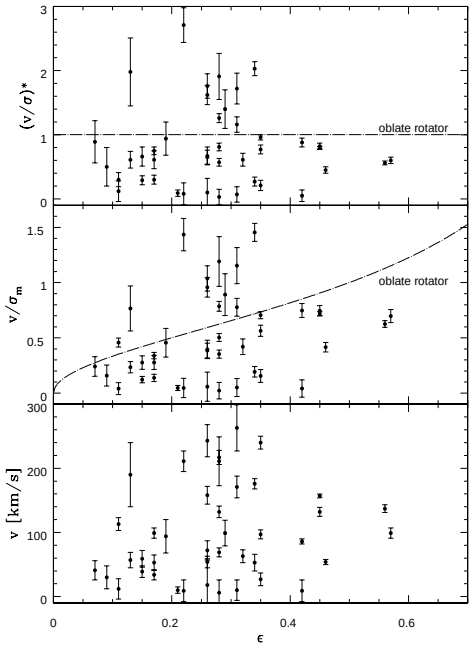

Fig. 1. $(v/\sigma)^*$ vs. ϵ, (v/σ) vs. ϵ and v vs. ϵ - diagrams. The dotted line represents the theoretical model of an oblate rotator

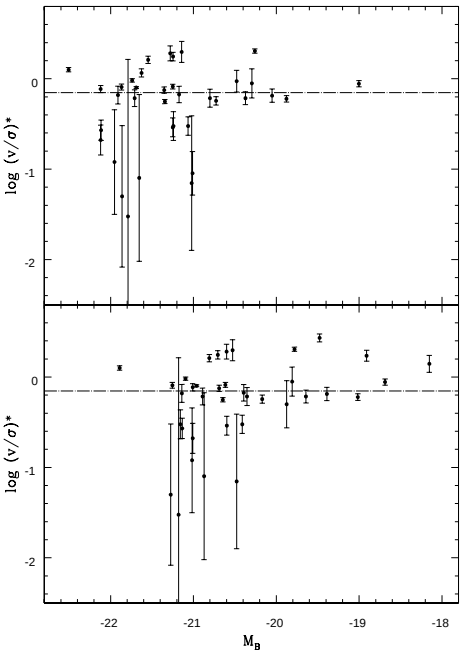

Fig. 2. The correlation between anisotropy and absolute luminosity in the B filter. The distances of the galaxies needed for the calculation of M_B were in the upper diagram taken from the catalog of Kraan-Korteweg (1986) and in the lower diagram derived under the assumption of an undisturbed Hubble flow. The dotted line represents the dividing line between rotational supported systems and anisotropic galaxies $(v/\sigma)^* = 0.7$ given by Bender et al. (1992)

The data point of one galaxy, NGC 6861, lies within the "zone of exclusion" (ZOE) $\kappa_1 + \kappa_2 > 8.0$ defined by Burstein et al. (1997). All galaxies are giant sequence (Gas-Stellar Continuum) members. In the giant sequence κ_2 increases while κ_1 decreases, it contains bulges, normal ellipticals (giant and intermediate) and compacts.

4.3. Statistics

Rotational velocity profiles, velocity dispersion profiles, h_3 and h_4-profiles were extracted for 49 galaxies. Bender et al. (1994) identified several kinematic types by their rotation, velocity dispersion, h_3 and h_4 profiles, finding correlations between kinematic profiles and photometric properties like diskyness or boxyness. Following this description, our sample galaxies were divided into the kinematic types, the kinematic types of the individual galaxies are listed in Table 6.

galaxies with decoupled central component kinematics	17 galaxies	= 32%
disky	7 galaxies	= 13%
boxy, without rotation	10 galaxies	= 19%
boxy, with weak rotation ...	3 galaxies	= 6%
E0	4 galaxies	= 8%
normal E-galaxies	7 galaxies	= 13%
unknown	3 galaxies	= 6%
not classifiable	9 galaxies	= 17%.

Galaxies where not enough data for this evaluation was obtainable are classified as "unknown", galaxies with profiles which did not fit into any of the representative object classes are found in "not classifiable". Some galaxies fit into more than one class, they are multiply counted.

Disky early-type galaxies are two-component systems with a hot bulge and a cold, fast rotating disk. This superposition will cause asymmetric LOSVDs which are characterized by strong negative h_3 values. Features in the major axis rotation curve that are caused by varying light contributions of the disk are reflected by similar features in the h_3 profile. Boxy ellipticals show none or only weak rotation and positive h_4 values on their major axes. Weak rotation causes some weak asymmetry in their LOSVDs and therefore slightly negative h_3 values. E0 galaxies do show a slight increase of velocity dispersion within their photometric core radii and smaller h_4 values inside their core radii than further out. Normal E-galaxies are galaxies with h_3 and $h_4 \approx 0$.

32% of all galaxies contain kinematically decoupled central components. The size of these central components was found to be 0.40 ± 0.28 kpc and in all cases less than 1 kpc. The identification of decoupled central components is based on the kinematic profiles, which show features typical for disky galaxies, but h_3 has the opposite sign

Table 6. Kinematic types of the sample galaxies following Bender et al. (1994)

galaxy	kinematic type	galaxy	kinematic type
I1729	disky:	N3302	boxy, without rotation:
N1404	decoupled central component	N3309	normal E-galaxy
N1427	decoupled central component	N3377	normal E-galaxy
N1537	normal E-galaxy	N3557B	decoupled central component
N1549	E0; boxy, with weak rotation	N3557	normal E-galaxy
N1889	unknown	N3585	decoupled central component; disky
N2271	decoupled central component; disky	N3617	decoupled central component:
N2325	not classifiable	N3260	disky
N2434	boxy, without rotation	N3636	E0; boxy, without rotation
N2380	boxy, without rotation	N3904	decoupled central component
I2311	decoupled central component; disky	N3923	not classifiable
U4508	not classifiable	N4033	decoupled central component
N2663	boxy, without rotation	N4105	decoupled central component
N2699	decoupled central component	N4106	unknown
N2887	boxy, without rotation	U7354	not classifiable
N2865	boxy, without rotation:	N4261	boxy, without rotation
N2872	unknown	N4697	normal E-galaxy
N2888	decoupled central component	N5061	E0; boxy, with weak rotation
N2986	decoupled central component	N5237	not classifiable
N3078	decoupled central component	N5903	boxy, without rotation
N3087	decoupled central component	I4797	disky
N3136	not classifiable	N6861	not classifiable
N3125	not classifiable	N7029	not classifiable
N3224	normal E-galaxy:	N7049	normal E-galaxy
N3250	decoupled central component:	N7196	decoupled central component:
N3258	boxy, with weak rotation	I5297	boxy, without rotation
N3268	disky		

to v and the reversal in the rotation corresponds to the radius where also h_3 changes sign. On comparing these galaxies with results in literature, a good accordance was found, e.g. NGC 3078 and NGC 3250 where central depressions in the Mg_2 profiles were identified by Carollo et al. (1993). For two of the sample galaxies central surface-brightness profiles have been obtained by HST, NGC 3377 and NGC 4697 (Faber et al. 1997). Both have power-law profiles which lack cores. NGC 4261 and NGC 4697 do contain nuclear dust structures also indentified by HST (van Dokkum & Franx 1995).

The percentage of sample galaxies where a disk component was evident is altogether 49%, in 36% no disk component could be detected and in 15% of the sample galaxies this is uncertain. It may therefore be concluded that more than half of the sample galaxies contain stellar disk components, adding the fact that with greater spatial resolution even smaller disks might have been detected.

The luminosity distributions of individual kinematic object classes are shown in Fig. 4. Galaxies with kinematically decoupled components are evenly distributed in the luminosity range, in contrary to Bender (1996) who find that these components should be more frequent in luminous ellipticals. The dichotomy in the class of elliptical galaxies in boxy and disky objects is confirmed also from the kinematic point of view. However it is noteworthy that some disky ellipticals show the signature of a kinematically decoupled central component.

It is an accepted fact that merging plays an important role in the evolution of early-type galaxies up to altering the original morphological type (Barnes 1996). The most notable signature of such an event are kinematically decoupled gaseous and stellar components (Bertola et al. 1990; Bender 1996). Statistics of our sample galaxies were used in order to verify this picture: ZCAT (Huchra et al. 1995) was searched for galaxies in the vicinity of each sample member using radial bins of 50, 100, 150 and 200 kpc around each galaxy and a redshift interval of ± 1000 km s^{-1}. The resulting histogram (Fig. 5) reflects the well-known fact that generally elliptical galaxies are located in high-density environments (Dressler et al. 1994). However, it is noteworthy that the subsample of objects with decoupled components are found in groups of even higher density than average.

The peculiar central component kinematics in some ellipticals can possibly also be explained in ways different from the above scenario. E.g. the decoupled component could be due to streaming in a triaxial body, obliquely projected (Binney 1985; Franx et al. 1991; Statler 1994); but rotation amplitudes in the central components are in general too high and central metallicities are enhanced with respect to the main body, so this scenario cannot

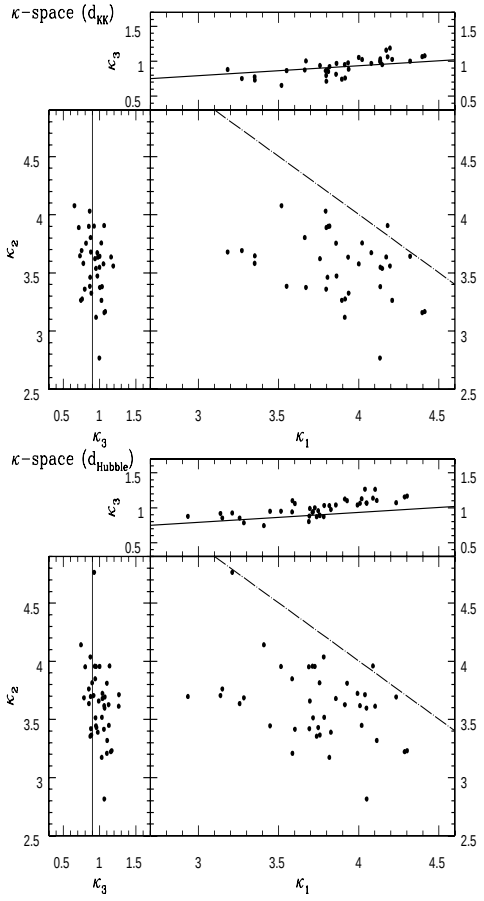

Fig. 3. κ-space in the parameterization published by Bender et al. (1992). The distances of the galaxies needed for the calculation of R_e were in the upper diagram taken from the catalog of Kraan-Korteweg (1986) and in the lower diagram derived under the assumption of an undisturbed Hubble flow. The dotted line in the κ_1/κ_2-plot marks the beginning of the "zone of exclusion" (ZOE), which extends to the upper right. The full line in the other projections marks the fundamental plane

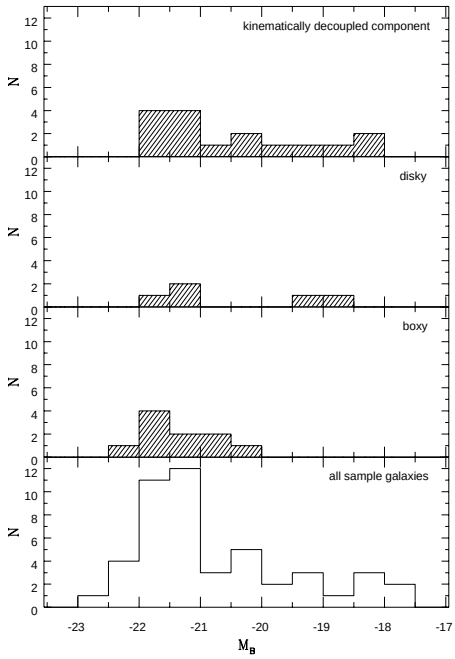

Fig. 4. Absolute luminosity distributions of the sample galaxies with respect to the kinematic types introduced by Bender et al. (1994). The shaded distributions represent respective luminosity distributions of the subsamples with kinematically decoupled component, boxiness or diskiness. Note that "diskiness" and "boxiness" were infered from the galaxy's kinematic profiles, not photometric properties

account for the formation of the majority of ellipticals with peculiar central components (Bender 1996).

5. Conclusions

We have measured the line-of-sight velocity distributions (LOSVDs) for a sample of 49 early-type galaxies by means of the fourier quotient method and the fourier fitting method. From the observed LOSVDs rotation velocities and velocity dispersions were derived and deviations of the LOSVDs from Gaussian profiles were parameterized by the amplitudes h_3 and h_4 of third- and fourth order Gauss-Hermite functions. For the investigation of correlations between different kinematic and photometric properties mean kinematic parameters were derived from the profiles.

The galaxies are shown to follow the general correlation between anisotropy and luminosity as described by Davies et al. (1983). The position of the galaxies in κ-space (Bender et al. 1992) was also plotted. All galaxies are shown to be giant sequence members, one galaxy lies within the zone of exclusion (ZOE).

Following Bender et al. (1994) the sample galaxies were divided into several representative object classes by examining their kinematic profiles. 32% of the examined galaxies contain kinematically decoupled central components, the size of these components was 0.40 ± 0.28 kpc, in each case the component was smaller than 1 kpc. The kinematic signature of a stellar disk component is found in 49% of the sample galaxies, in 15% this is uncertain. Therefore it is highly probable that in more than half of all early-type galaxies a stellar disk component exists.

The galaxies which contain kinematically decoupled components are more likely to be found in groups of higher density than others. This fact supports the theory that kinematically decoupled components are the remnants of merging events which are more likely to be found in high-density environments than in the field.

References

Barnes J., 1996, "Interaction and Induced Star Formation", Saas-Fee Advanced Course 26, Lecture Notes 1996, p. 275
Bender R., Surma P., 1992, A&A 258, 250

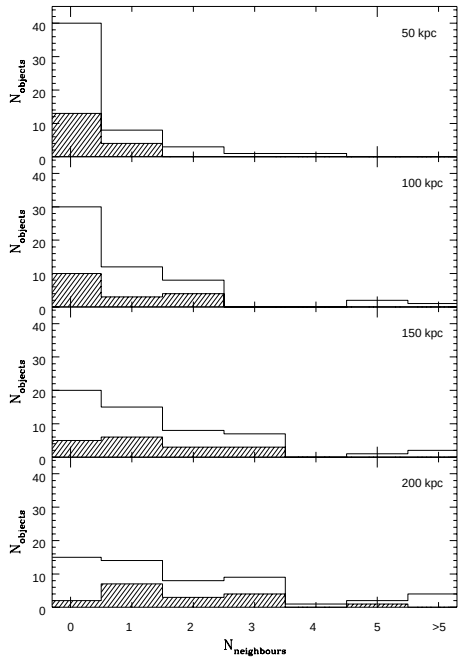

Fig. 5. Histograms of the number of sample galaxies with neighbours within a redshift interval of ± 1000 km s^{-1} using ZCAT. The histograms range from a radial distance between sample galaxies and neighbours from $0 < r < 50$ kpc (uppermost diagram) to $150 < r < 200$ kpc (lowest diagram). The histograms for sample galaxies with kinematically decoupled components are shown as shaded. The last $N_{\rm neighbour}$ bin includes all galaxies with more than 5 nearby galaxies. A trend that galaxies with kinematically decoupled components are more likely to be located in crowded environments (where $N_{\rm neighbours}$ is higher) is evident

Bender R., Burstein D., Faber S.M., 1992, ApJ 399, 462
Bender R., Saglia R.P., Gerhard O.E., 1994, MNRAS 269, 785
Bender R., 1996, IAU Symp. 171 "New Light on Galaxy Evolution", Bender R., Davies R.L. (eds.). Kluwer, Netherlands, p. 181
Bertola F., et al., 1990, "Dynamics and Interactions of Galaxies", Wielen (ed.), p. 249
Binney J.J., 1978, MNRAS 183, 501
Binney J.J., 1985, MNRAS 212, 767
Binney J.J., Davies R.L., Illingworth G.D., 1990, ApJ 361, 78
Burstein D., Davies R.L., Dressler A., et al., 1987, ApJS 64, 601
Burstein D., Bender R., Faber S.M., Nolthenius R., 1997, AJ 114, 1365
Campos-Aguilar A., Moles M., 1991, A&A 241, 358
Carollo C.M., Danziger I.J., Buson L., 1993, MNRAS 265, 553
Carollo C.M., Danziger I.J., 1994a, MNRAS 270, 523
Carollo C.M., Danziger I.J., 1994b, MNRAS 270, 743
Danziger I.J., Goss W.M., 1983, MNRAS 202, 703
Davies R.L., et al., 1983, ApJ 266, 41
Dejonghe H., et al., 1996, A&A 306, 363
de Vaucouleurs G., de Vaucouleurs A., Corwin H.G., et al., 1991, "Third Reference Catalogue of Bright Galaxies". Springer Verlag (RC3)
Dressler A., Oemler A., Butcher H.R., Gunn J.E., 1994, ApJ 430, 107
Faber S.M., Wegner G., Burstein D., et al., 1989, ApJS 69, 763
Faber S.M., Tremaine S., Ajhar E.A., et al., 1997, AJ 114, 1771
Franx M., Illingworth G., Heckman T., 1989, ApJ 344, 613
Franx M., Illingworth G., de Zeeuw T., 1991, ApJ 383, 112
Huchra J.P., Geller M.J., Corwin H.G., 1995, "The CfA Redshift Catalogue", Harvard-Smithsonian Center for Astrophysics (ZCAT)
Kraan-Korteweg R.C., 1986, A&AS 66, 255
Lauberts A., Valentijn E.A., 1989, "The Surface Photometry Catalogue of the ESO-Uppsala Galaxies", ESO, ESO-Uppsala
Liu C.T., Kennicutt R.C., 1995, ApJ 450, 547
Marlowe A.T., Meurer G.R., Heckman T.M., Schommer R., 1997, ApJS 112, 285
Papaderos P., Loose H.-H., Thuan T.X., Fricke K.J., 1996, A&AS 120, 207
Paturel G., Fouque P., Bottinelli L., Gouguenheim L., 1989, A&AS 80, 299, "Catalogue of Principal Galaxies" (PGC)
Reduzzi L., Rampazzo R., 1996, A&AS 116, 515
Sadler E.M., Jenkins C.R., Kotanyi C.G., 1989, MNRAS 240, 591
Sandage A., Tammann G.A., 1981, "Revised Shapley-Ames Catalog of Bright Galaxies". Carnegie Institution of Washington Publications, p. 635 (RSA)
Slee O.B., Sadler E.M., Reynolds J.E., Ekers R.D., 1994, MNRAS 269, 928
Statler T.S., 1994, ApJ 425, 500
Telles E., Melnick J., Terlevich R., 1997, MNRAS 288, 78
Thomson R.C., 1992, MNRAS 257, 689
van der Marel R.P., Franx M., 1993, ApJ 407, 525
van Dokkum P.G., Franx M., 1995, AJ 110, 2027

Appendix A: Kinematic profiles of the sample galaxies

Shown here are the kinematic profiles of all sample galaxies with absorption lines strong enough for fourier fitting[7]. The profiles were obtained by applying the fourier fitting method with Gauss-Hermite polynomials on the sample spectra. The graphs plot rotational velocity, velocity dispersion, h_3 and h_4 values as a function of the distance from the centers of intensity. Filled and open circles refer to opposite sides from the centers. The spatial direction of the galaxy's side where the filled circles point to is given at the upper right corners of the plots. Distances from the centers are given in arcseconds below the plots and in units of the effective radii, when available (see Table 1), on top of the plots. The position angle of the slit was generally aligned with the optical major axis of the target galaxy, with the exceptions of NGC 2663 and NGC 4697, where two different position angles where used.

[7] Only the first page of Fig. 6 is printed, the full figure is available at http://www.edpsciences.org

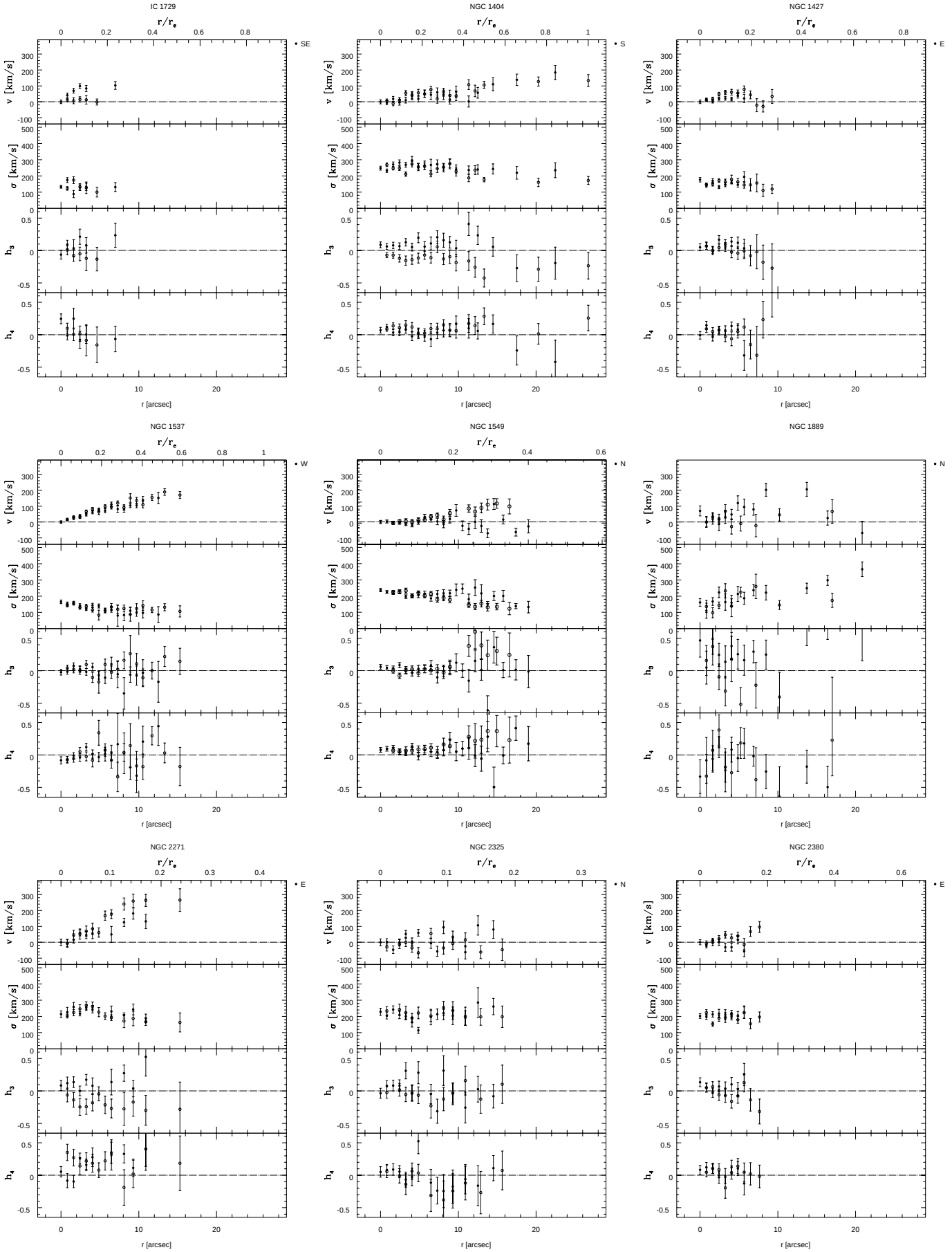
IC 1729
NGC 1404
NGC 1427
NGC 1537
NGC 1549
NGC 1889
NGC 2271
NGC 2325
NGC 2380
r/r_e
v [km/s]
σ [km/s]
h_3
h_4
r [arcsec]

Fig. 6.